Acceleration mechanism of abrasive particle in ultrasonic polishing under synergistic physical vibration and cavitation: Numerical study

Xin Chen [a,b,1], Shucong Xu [c,1], Juan Ignacio Ahuir-Torres [b], Zixuan Wang [a], Xun Chen [b], Tianbiao Yu [a,*], Ji Zhao [a,*]

[a] School of Mechanical Engineering and Automation, Northeastern University, Shenyang 110819, China
[b] Faculty of Engineering and Technology, Liverpool John Moores University, Liverpool L3 3AF, UK
[c] School of Materials Science and Engineering, Harbin Institute of Technology, Harbin 150001, China

ARTICLE INFO

ABSTRACT

Ultrasonic technology is widely applied in the engineering ceramic polishing processes without the limitation of material properties and ideally integrated into computer numerical control system. Ultrasonic-induced cavitation and mechanical vibration effect could accelerate the motion of solid abrasives. The individual behaviors of microjet/shockwave of ultrasonic cavitation in gases and liquids, and micro-abrasives with simple harmonic vibrations in solids and liquids has been extensively studied. To conduct a systematic and integrated study of abrasives behavior in the polishing contact region involving abrasive, surround-workpiece wall, ultrasonic physical vibration, and ultrasonic cavitation impact, a novel model integrating the free abrasive motion velocity and fixed abrasive indentation depth under multi-scale contact was proposed according to Hertzian contact theory, Greenwood-Williamson model, indentation deformation theory, the basic equations of cavitation bubble dynamics, cavitation impact control equations, and Newton's law of motion equation. The effects of ultrasonic amplitude, ultrasonic frequency, preloading force and particle size on the proposed model were investigated by theoretical analysis and numerical simulations. Ultrasonic physical vibration mainly influences the dynamic gap and further influence the number of different abrasives. Furthermore, the indentation depth of fixed abrasive depends mainly on the abrasive geometry. As the contact gap and abrasive size decrease, the indentation depth gradually decreases. Under the synergistic effect of cavitation-induced shock wave and microjet, the velocity of free abrasive in this paper is generally 0–150 m/s, and the kinetic energy of free abrasive increases roughly linearly with increasing frequency and approximately as a quadratic function with increasing particle size. Increasing the preloading force leads to a reduction in the abrasive kinetic energy. Besides, the kinetic energy induced by the shock wave has a cliff-like increment at an amplitude of 0.7–0.8 μm. It is revealed that the abrasive kinetic energy is suppressed by the cavitation bubble expansion and collapse at smaller ultrasonic pressure amplitude and surround-wall distance. This research provides a theoretical reference for the modeling of potential defects and material removal on the workpiece surface caused by abrasive motion during polishing, and reduces the trial cost for parameter optimization in actual polishing processing.

1. Introduction

Polishing has been renowned as an advanced precision process where slow work yields delicate products. It is widely used in the finishing processing of engineering ceramics, multifunctional crystals, optical glasses, semiconductor wafers, ceramic matrix composites, and other difficult to machine materials. However, due to the characteristics of high hardness and low fracture toughness of these types of materials as well as the industrial challenge of increasing productivity, ultrasonic vibration technology is applied to the polishing processes as it is not limited by material properties and is ideally integrated into computer numerical control systems [1]. Ultrasonic, a kind of super-high frequency vibration, propagates in the medium and produces ultrasonic effects, including cavitation effect, acoustic flow and mechanical

vibration [2]. These effects can accelerate the motion of solid abrasives to achieve greater mechanical removal. In the past few decades, extensive experimental and theoretical research has been developed on the individual behaviors of microjet/shockwave of ultrasonic cavitation in gas and liquid, and micro-abrasives with simple harmonic vibrations in solids and liquids, however, there is a lack of integrated investigation of the synergistic effects of ultrasonic cavitation and mechanical periodic vibrations on solid abrasives in polishing systems where gas, liquid and solids come together.

Yu et al., [3] compared the differences between conventional mechanical polishing and ultrasonic vibration-assisted polishing for single crystal silicon processing. They reported that ultrasonic vibration can effectively improve the material removal rate and quickly achieve a superior surface quality. It may be because the ultrasonic action caused an increase in the contact area of abrasives, thus enabling a significant increase in the polished volume. Yang et al., [4] applied ultrasonic vibration assisted electro-chemical mechanical polishing to achieve sub-nanometer roughness of single-crystal silicon carbide. They found that ultrasonic vibration improved the anodic oxidation rate and increased the material removal rate to approximately 4.5 times that of electro-chemical mechanical polishing. Tsai et al., [5] developed an ultrasonic vibration-assisted chemical mechanical polishing (UV-CMP) method to investigate the effect of ultrasonic vibration on copper substrates polishing. It is indicated that UV-CMP has a 50 % increase in the material removal rate relative to traditional chemical mechanical polishing. Sihag et al., [6] deigned and fabricated an ultrasonic assisted magnetic abrasive finishing system for finishing tungsten. They stated that ultrasonic vibrations could increase the interaction of abrasive particle cutting edges with the surface wave crest. Srivastava and Pandey [7,8] applied the longitudinal ultrasonic vibrations into the double-disc chemical assisted magnetorheological finishing of silicon wafers. They concluded that ultrasonic power has a more significant effect on material removal that other factors such as polishing speed and abrasive concentration. Xu et al., [9] used ultrasonic flexural vibration to assist chemical mechanical polishing of sapphire. They indicated that the contact path length, the contact force, and the impaction between the silica particles and the sapphire surface can be increased with the aid of ultrasound from the kinematics and dynamics point of view. Deng et al., [10] also proved that the same technique as Xu et al., [9] is feasible to improve the machining quality of sapphire. Choopani et al [11] proposed an ultrasonic assisted-rotational magnetorheological abrasive flow finishing process for the aluminum 2024 tubes. Result showed that the percentage improvements in surface roughness and material removal were 94.57 % and 0.0514 % with ultrasonic and 87.4 % and 0.0281 % without ultrasonic. Baghel et al., [12] presented an ultrasonic vibration-assisted magnetorheological finishing (VAMRF) process on the glass optics. Result showed that hybrid VAMRF provided approximately 20 % higher material removal rate as compared to that of conventional magnetorheological finishing. The investigations of the above scholars have well demonstrated that the improvement of ultrasonic vibration in solids and liquids two-phase flow for physical scratching of abrasives largely stems from the periodic simple harmonic vibration presented by polishing tools in the region of 2 times of ultrasonic amplitude.

In addition, numerous studies revealed that the overall erosion can be enhanced when abrasives are employed in the cavitation flow of gas and liquid. Considerable work [13–24] has been carried out to obtain an understanding of the complicated interactions between cavitation and abrasives and the synergistic effects on erosion. Tan and Yeo [20,21] showed that ultrasonic cavitation abrasive finishing can remove the finest fractional melted powders on the surface of additive manufactured components, and further reduce the final *Ra* to 3.5–3.8 μm, with side surface roughness improvement of up to 45 %. Kumar et al., [22] used ultrasonic cavitation accelerated alumina abrasives to investigate the micro-deburring process and mechanism of micro-milled difficult-to-machine materials. The results show that for soft materials such as

aluminum 6061 and copper, the burr was reduced by 92 % in a very short time of ten seconds, and for titanium alloy and bearing steel, the burr was reduced by three to six minutes without damaging the part or causing any deterioration in dimensional accuracy. 10 s of micro-deburring resulted in a reduction in channel surface roughness from 8.97 nm to 6.63 nm and a 26 % increase in surface finish. Peng et al., [23] conducted ultrasonic cavitation micro-abrasive erosion of reservoir rocks in distilled water incorporating silicon dioxide micro-abrasives with an average diameter of 0.5 μm and a mass concentration of 1–7 wt%. They pointed out that the addition of silicon dioxide micro-abrasives resulted in increased mass removal of 81.41 % for sandstone, 557.38 % for shale, and 188.16 % for granite. Farbod and Pourabbas [24] investigated the effect of ultrasonic wave at the interface between water and silica nanoparticles on the erosion, abrasion and wear of polymethyl methacrylate surfaces. They stated that such nanoparticles not only exacerbate erosion but also act as abrasive particles in a manner similar to the abrasive jet processing technique. In addition, surface embedding of nanoparticles was also observed, which can be seen as a new method for surface decoration and property modification. Ge et al., [25] proposed an ultrasonic coupled abrasive jet polishing method for glass-based micro-channel and indicated that ultrasonic could obviously increase the turbulent kinetic energy and impact erosion to improve the jet stability and polishing efficiency. Liu et al., [26] proposed the electrorheological (ER) fluid–assisted ultrasonic polishing method to improve surface finish of metal additive manufacturing parts. Result showed that the average surface roughness is reduced from 5.6 μm to 2.74 μm after 20 min polishing. The material removal in the polishing process is mainly based on the cavitation impact and the abrasive grinding action. Laguna-Camacho et al., [18] performed ultrasonic cavitation erosion experiments with and without silicon carbide abrasives particles of the same size on pure aluminum and steel 1045. The findings indicated that abrasive particles can be observed to move along both surfaces and stay in the gap, thus causing higher wear damage to both surfaces. The wear mechanism was identified using optical microscopy and was characterized by a pitting action with the use of deionized water only, while scratches and irregular indentations could be observed on the surfaces cavitated in deionized water with abrasive particles. Chen et al., [13] compared the erosion of metal specimens by adding spherical and irregular micro-abrasives into deionized water. The findings showed that water containing micro-abrasives had a greater erosive action.

Based on the above literature survey, a systematic and integrated study of abrasive behavior in the polishing contact region involving abrasive, surround-workpiece wall, ultrasonic physical vibration, and ultrasonic cavitation impact is unprecedented. This paper proposes a model integrating the free abrasive motion velocity and fixed abrasive embedding depth under multi-scale contact. Hertzian contact theory and Greenwood-Williamson (GW) model with probability density are used to describe the asperity and micropore of contact between polishing pad and workpiece, and further determine the movement mode of abrasives in the polishing slurry; Indentation deformation theory and Hertzian contact large deformation theory are used to calculate the indentation depth of fixed abrasive; The basic equations of cavitation bubble dynamics, cavitation impact control equations, and Newton's law of motion equation of abrasive particle are used to calculate the motion velocity and kinetic energy of free abrasive. The effects of dominant ultrasonic factors and processing parameters on the proposed model are investigated by theoretical analysis and numerical simulation. This provides a theoretical reference for the modeling of potential defects and material removal on the workpiece surface caused by abrasive motion during polishing, and reduces the trial cost for parameter optimization in actual polishing processing.

2. Theory and methodology

A two-dimensional schematic of actual experimental ultrasonic

polishing (UP) system is shown in Fig. 1, which consisted mainly of a slurry unit, a polishing tool unit coupled with ultrasonic vibration and a workpiece unit fixed to the workbench. The used workpiece is SiC ceramic with some difficult-to-machine properties of hard and brittle. To mitigate potential defects such as scratches on polished surfaces, a polyurethane pad is used as the polishing tool owing to its softness and porosity improving the three-body abrasion ratio of abrasives and minimizing damage to the workpiece. The slurry unit provides a great deal of super-hard abrasives for interaction between the workpiece and the polishing pad, as shown in Fig. 1(B). The small size abrasives show two main contact states in the contact area, namely the fixed state and the free state. Besides, as the main feature of this polishing technology, ultrasonic electro-spindle provides axial ultrasonic vibration for the

polishing tool and ultrasonic cavitation effect for the polishing slurry. In order to explore the contact and kinetic geometry of abrasive particles, multi-scale contact models of workpiece, polishing pad, abrasives and polishing slurry are established.

2.1. Contact model between workpiece and pad

The adopted polishing tool base is made of red corundum, so that the polyurethane pad can be regarded as an elastomer compared to red corundum and silicon carbide, which means the tool base and the workpiece can be regarded as rigid bodies. When the cylindrical polishing pad is pressed on the workpiece surface, the produced elastic deformation of polishing pad during contact is much larger than that of
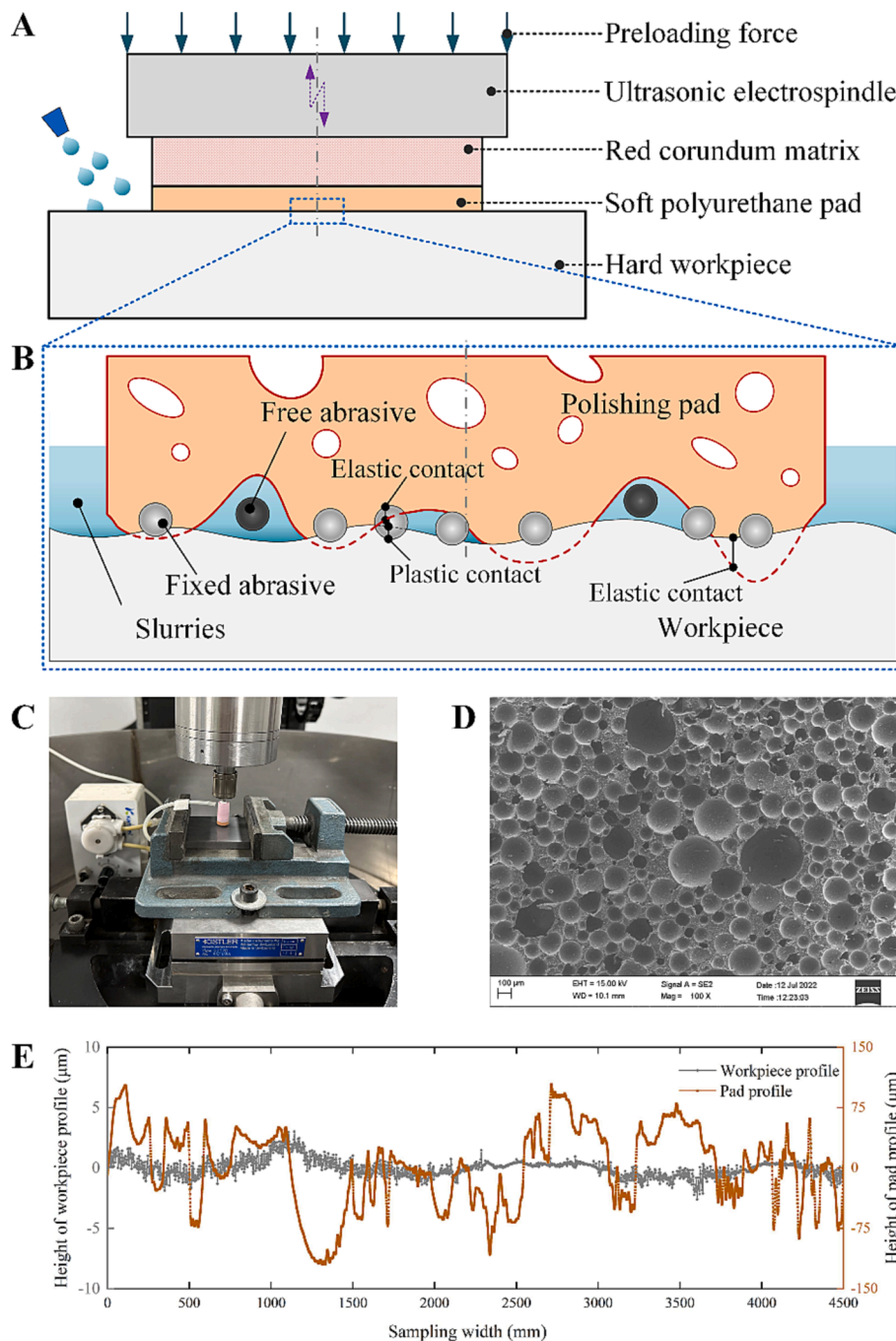

Fig. 1. Two-dimensional schematic (A) and actual experimental setup (C) of ultrasonic polishing system; contact states (B) of fixed and free abrasive particles between soft polishing pad and hard workpiece; microscopic morphology (D) of polishing pad; the surface profile (E) of the as-received workpiece and polishing pad.

the workpiece materials [27]. At the millimeter scale, the size of abrasive particles and the down load from the polishing fluid flow on the workpiece surface are negligibly small, so the contact between the polishing pad and the workpiece can be simplified to a Hertzian contact between a thin elastic cylindrical bottom surface and a semi-infinite rigid plane [28]. The compression depth of polishing pad is defined as the ideal distance that the pad would penetrate the workpiece if the workpiece plane was not rigid. In accordance with the Hertzian contact theory, the maximum compression depth without ultrasonic vibration can be expressed as

$$\delta_p = \frac{F_0 L}{\pi R_p^2 E_p} \tag{1}$$

where, L and R_p are the thickness and radius of polishing pad respectively; E_p is the Young's modulus of polishing pad; and δ_p is the static compression depth of polishing pad when the preloading force is F_0.

Further, as the ultrasonic vibration amplitude belongs to the micron level, the ultrasonic vibration-induced position change of polishing pad is temporarily excluded from the influence of its elastic deformation, and the dynamic compression depth $\delta_p(t)$ of polishing pad can be

calculated as:

$$\delta_p(t) = \frac{F_0 L}{\pi R_p^2 E_p} + A\sin(2\pi ft + \varphi_0) \tag{2}$$

where, A, f and φ_0 are the ultrasonic amplitude, frequency, and initial phase, respectively. t is the time. The suffix (t) in the latter context all denotes the dynamic variation value with t under the ultrasound action. Substituting the Eq. (2) into Eq. (1), the dynamic polishing force $F_d(t)$ under ultrasonic vibration can be computed as:

$$F_d(t) = F_0 + \frac{\pi R_p^2 E_p A\sin(2\pi ft + \varphi_0)}{L} \tag{3}$$

2.2. Contact model between workpiece and asperities

At the micrometer scale, Fig. 1(D) exhibits that the surface of polishing pad consists of dense micro-pores and asperities, thus the actual contact surface between the pad and the workpiece is tiny asperities surface on the non-porous areas, as shown in Fig. 1(E). The surface roughness value of original polishing pad and workpiece are 53.6 μm and 485 nm, respectively. Compared to the roughness and local profile
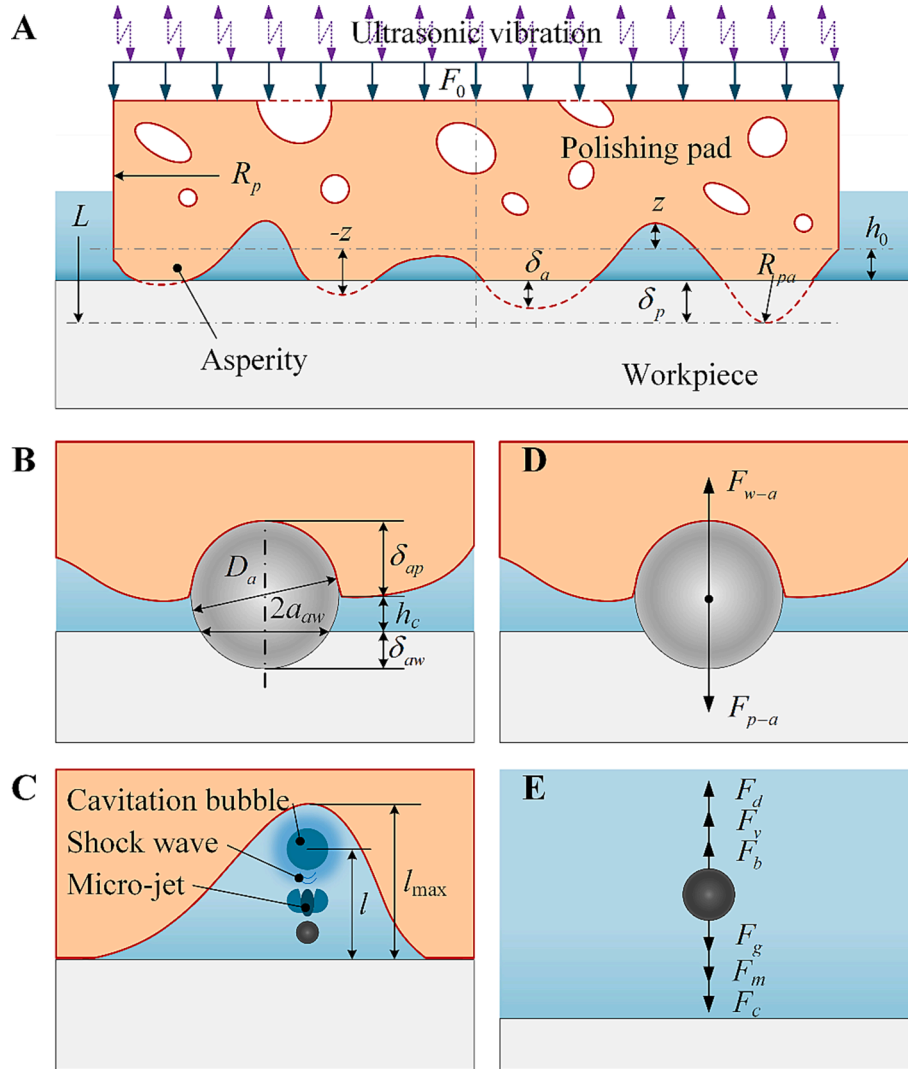

Fig. 2. Contact geometry (A) between soft polishing pad and hard workpiece according to Greenwood-Williamson model; contact geometry (B) and force analysis (D) of single fixed abrasive particle between soft polishing pad and hard workpiece, the forces acting on the single fixed abrasive particle includes the contact force F_{w-a} from the workpiece and the elastic contact force F_{p-a} from the pad; kinetic geometry (C) and force analysis (E) of single free abrasive particle in the polishing slurry under ultrasonic cavitation, the forces acting on the single free abrasive particle includes cavitation force (F_c), pressure drag (F_d), viscosity resistance (F_v), virtual mass force (F_m), gravity (F_g) and buoyancy (F_b).

of both, the workpiece surface can be simplified to a relatively smooth surface, while the surface profile of the polishing pad is to be considered realistically. Fig. 2(A) shows the contact geometry between soft polishing pad and hard workpiece. Greenwood-Williamson (GW) [29] proposed a mathematical model to describe the contact of a rough surface, which is widely used to solve the contact problem in polished areas. In the GW model, all asperities on the polishing pad are simplified as spheres with the same radius of curvature R_{pa}. The height of the asperities follows the normal distribution according to the research [30],

$$\varphi(z) = \left(\frac{1}{2\pi R_{qp}^2}\right)^{1/2} e^{\frac{-z^2}{2R_{qp}^2}} \tag{4}$$

where, z is the height coordinate of an asperity, and $z = 0$ represents the average height of polishing pad's profile. R_{qp} is the root mean square of the height distribution.

The elastic deformation of asperities occurs on the workpiece surface when the pad is compressed. Using the Hertzian contact theory, the force of single asperity $F_{pa}(t)$ can be described as:

$$F_{pa}(t) = \frac{4}{3} E_{pw} R_{pa}^{1/2} \delta_a(t)^{3/2} \tag{5}$$

where, R_{pa} is the radius of an asperity, $\delta_a(t)$ is the dynamic penetration depth of an asperity, which can be expressed according to the height z of the asperity and a dynamic average distance $h_0(t)$ between the average height of polishing pad's profile and that of workpiece.

$$\delta_a(t) = -z - h_0(t) \tag{6}$$

E_{pw} denotes the equivalent elastic modulus of the polishing pad and the workpiece, expressed as:

$$E_{pw} = \left(\frac{1 - \nu_p^2}{E_p} + \frac{1 - \nu_w^2}{E_w}\right)^{-1} \tag{7}$$

where, E_w is the Young's modulus of the workpiece, ν_p and ν_w are the Poisson ratio of the polishing pad and workpiece, respectively.

The total number N_{pc} of asperities that come into contact with the workpiece is expressed as:

$$N_{pc} = N_{pa} \int_{-\infty}^{-h_0(t)} \varphi(z) dz \tag{8}$$

$$N_{pa} = \pi R_p^2 \rho_{pa}^2 \tag{9}$$

where, N_{pa} defines the total number of asperities on the nominal area of polishing pad, which can be expressed as the product of the nominal area of polishing pad and the linear density ρ_{pa} of asperities.

Integrating Eqs. (3)–(9) based on the fact that dynamic polishing force is mainly undertaken by all asperities of polishing area to obtain Eq. (10) for solving the dynamic average gap $h_0(t)$ under the specified polishing force.

$$F_0 + \frac{\pi R_p^2 E_p A \sin(2\pi ft + \varphi_0)}{L} =$$
$$\frac{4}{3} E_{pw} R_{pa}^{1/2} \left(\frac{1}{2\pi R_{qp}^2}\right)^{1/2} \pi R_p^2 \rho_{pa}^2 \int_{-\infty}^{-h_0(t)} e^{\frac{-z^2}{2R_{qp}^2}} (-z - h_0(t))^{3/2} dz \tag{10}$$

2.3. Interaction model of fixed abrasive between workpiece and pad

At the nanometer scale, it becomes important to investigate the interaction between the abrasive, the asperities, the workpiece and the polishing slurry. Abrasives exhibit two contact states depending on the contact gap between the asperities and the workpiece. When an axial ultrasonic vibration is applied to the polishing tool, the penetration depth of the fixed abrasives into the workpiece will directly determine

the progress of material removal. In order to simplify the model, the modelling process can be assumed that the abrasive is spherical rigid body and does not undergo any deformation, ignoring the interaction between the abrasives, and considering only the case where the polishing tool is subjected to ultrasonic vibration. Fig. 2(B, D) illustrates the contact geometry and force analysis of single fixed abrasive particle between soft polishing pad and hard workpiece.

Considering that the pad does not rotate, the fixed abrasive is embedded between the asperity of polishing pad and the workpiece when the contact gap h_c is very small. Due to the soft behavior of the pad, the fixed abrasive is embedded into the pad at a significant distance, which represents a big elastic deformation issue. According to its relevant theory [31,32], the elastic contact force F_{p-a} acting on single fixed particle from the pad is expressed as,

$$F_{p-a} = \frac{4}{3} E_{ap} R_a^{1/2} \delta_{ap}(t)^{3/2} + 5 R_a^{-3/20} \delta_{ap}(t)^{43/20} \tag{11}$$

where, E_{ap} denotes the equivalent elastic modulus of the polishing pad and the abrasive, R_a is the abrasive radius, $\delta_{ap}(t)$ is the compression depth of abrasive into the pad.

Considering the high hardness properties of the workpiece, the indentation depth of abrasive into the workpiece is much smaller than the abrasive diameter, which represents a dynamic indentation deformation issue [33]. According to the wear mechanics, the indentation depth $\delta_{aw}(t)$ and the contact force F_{w-a} acting on single fixed particle from the workpiece can be expressed respectively as,

$$F_{w-a} = H_w A_{aw} = H_w \pi a_{aw}(t)^2 \tag{12}$$

$$a_{aw}(t) = \sqrt{(D_a - \delta_{aw}(t)) \cdot \delta_{aw}(t)} \approx \sqrt{D_a \cdot \delta_{aw}(t)} \tag{13}$$

$$h_c = D_a - \delta_{aw}(t) - \delta_{ap}(t) \tag{14}$$

where, H_w is the hardness of the workpiece, D_a is the abrasive size. $a_{aw}(t)$ is the radius of the contact zone between a single abrasive and workpiece. Further, according to the force balance of the fixed abrasive, the indentation depth of abrasive into the workpiece can be calculated by solving Eq. (15).

$$\frac{4}{3} E_{ap} R_a^{1/2} (D_a - \delta_{aw}(t) - h_c)^{3/2} + 5 R_a^{-3/20} (D_a - \delta_{aw}(t) - h_c)^{43/20} =$$
$$H_w \pi D_a \cdot \delta_{aw}(t) \tag{15}$$

2.4. Interaction model of free abrasive in polishing slurry

At the nanometer scale, another key consideration is the motion state of free abrasive induced by the ultrasonic cavitation effect of polishing slurry in the micro-pores area of polishing pad, as shown in Fig. 2(C). Since the maximum micro-pore depth belongs to the micron scale, ultrasonic wave will interfere with the workpiece, which is a typical surround-wall ultrasonic cavitation issue. Considering the effects of the weak compressibility, viscosity and surface tension of polishing slurry and the rigid workpiece wall on the bubbles, the cavitation bubble dynamics model is modified on the typical Rayleigh-Plesset model and can be expressed as,

$$P_{out} = P_{\infty} + \frac{2\sigma}{R} + \frac{4\mu \dot{R}}{R} = P_s \sin(2\pi ft) + P_0 + \frac{2\sigma}{R} + \frac{4\mu \dot{R}}{R} \tag{16}$$

$$P_{in} = P_v + P_g = P_v + (kP_0 - P_v + \frac{2\sigma}{R_0})(\frac{R_0^3 - h_i^3}{R^3 - h_i^3})^\gamma \tag{17}$$

$$R\ddot{R} + \frac{3}{2}(\dot{R}^2 + v^2) + \frac{1}{2l} \frac{d(R^2 \dot{R})}{dt} = \frac{P_{in} - P_{out}}{\rho_s} + \frac{R}{\rho_s c_s} \frac{d(P_g - P_s \sin(2\pi ft))}{dt} \tag{18}$$

where, R_0, R, $\dot{R}$ and $\ddot{R}$ are the initial and actual radii of cavitation bubble and its corresponding first-order and second-order derivatives with

respect to time t, l is the vertical distance between the sphere center of cavitation bubble and the wall, P_v and P_g are the saturated vapor pressure and instantaneous partial pressure inside the bubble, respectively, P_∞ and P_0 are the environment pressures and static partial ambient pressure. σ and μ are the surface tension coefficient and viscosity coefficient of the slurry, γ and k are the polytropic exponent and variation coefficient of gas. h_i is the van der waals radius of cavitation bubble. v is the pad rotational velocity.

When the high intensity ultrasonic vibration at the bottom of polishing pad is transmitted to the polishing fluid medium mixed with bubbles and abrasives, it will drive the polishing fluid to produce cavitation effect, thus the ultrasonic sound pressure amplitude of polishing slurry propagated from the polishing pad can be expressed as,

$$P_s = \frac{2P_p \rho_s c_s}{\rho_s c_s + \rho_p c_p} = \frac{4\pi f A \rho_p c_p \rho_s c_s}{\rho_s c_s + \rho_p c_p} \tag{19}$$

where, ρ and c are the density and sound velocity respectively, and the subscripts of s and p represent the polishing slurry and the pad tool respectively. A and f are the ultrasonic amplitude and frequency, respectively. P_p is the ultrasonic sound pressure amplitude of polishing pad tool.

Substituting the Eqs. (16)–(17) and (19) into Eq. (18), the variation trend of cavitation bubbles in the ultrasonic sound field can be solved in MATLAB software. As is well-known, cavitation bubbles form, grow, implode and finally collapse to produce the cavitation effect impact in the polishing slurry under the action of ultrasonic waves.

However, the presence of abrasives into the cavitating slurry alters the damage rate of the workpiece, which is frequently attributed to the synergistic effect of cavitation and solid abrasive collisions [44,45]. In order to reveal the systematic mechanism, an interaction model between the impact kinetic energy of free abrasive and the impact of the cavitation effect will be established in this paper. In the vertical direction, according to Newton's second law of motion [46], the following relationship exists between the combined force on the abrasive and the corresponding acceleration in the force direction, as shown in Fig. 2(E).

$$\frac{1}{6}\pi \rho_a d_a^3 \dot{v}_a = \sum F_l \tag{20}$$

where, F_l represents the longitudinal component force, including the cavitation force (F_c), pressure drag (F_d), viscosity resistance (F_v), virtual mass force (F_m), gravity (F_g) and buoyancy (F_b). ρ_a and d_a are the density and size of abrasive, respectively, as well as the subscript a represents the abrasive.

$$F_c = P_c S \tag{21}$$

$$F_v = 3\pi \mu d_a v_a \tag{22}$$

$$F_d = C\rho_s v_a^2 S / 2 \tag{23}$$

$$F_b = \rho_s g V_a \tag{24}$$

$$F_g = m_a g \tag{25}$$

$$F_m = -\frac{1}{2}V_a \rho_s \dot{v}_a \tag{26}$$

where, P_c is the cavitation effect impact pressure, S is the force area of abrasive, v_a and $\dot{v}_a$ are the abrasive particle velocity and its first-order derivative with respect to time t. V_a and m_a are the volume and mass of abrasive, respectively. g is the gravitational acceleration. C is the resistance coefficient.

Due to the influence of abrasives in the polishing slurry and the workpiece wall, cavitation effects in the form of microjet and shock wave [47] will be generated and act on the surface of abrasive particle during the collapse of bubbles to give it a certain amount of impact

kinetic energy. Therefore, the cavitation effect impact pressure P_c was considered into two types, namely, the shock wave pressure (P_s) and microjet pressure (P_j). The bubble collapse process proceeds very quickly [48], and can be completed in a few hundred nanoseconds in general, therefore it is defined as no significant heat exchange between the bubble and the surrounding polishing slurry. The motion velocity of cavitation bubble wall during the collapse of bubble was obtained according to the conservation of energy with respect to the interaction of the cavitation bubble and the polishing slurry.

$$\dot{R}^2 = \frac{2P_0}{3\rho_s(\gamma-1)}[(\frac{R_0}{R})^{3(2-\gamma)} - (\frac{R_0}{R})^3] + \\ \frac{2\sigma}{\rho_s R_0}[(\frac{R_0}{R})^3 - \frac{R_0}{R}] - \frac{2(P_\infty - P_v)}{3\rho_s}[(\frac{R_0}{R})^3 - 1] \tag{27}$$

Brujan et al., [49–51] utilized high-speed photography to capture the shock wave front formed after bubble rupture and further extracted its propagation velocity. And its relationship with the motion velocity of the cavitation bubble wall was summarized, which can be expressed as

$$v_s = k_2 \lg(\frac{\dot{R} + k_1}{k_1}) + c_s \tag{28}$$

Associating Eqs. (27) and (28) to obtain the velocity of shock wave and further calculate the pressure of shock wave according to the literature [52].

$$P_s = k_1 \rho_s v_s (10^{\frac{v_s - c_s}{k_2}} - 1) + P_\infty \tag{29}$$

Where, k_1 and k_2 are the experimental fit coefficients, v_s is the velocity of shock wave.

Asymmetric collapse occurs when a bubble is subjected to an uneven pressure, the microjet can be generated and oriented towards the abrasive particle surface [53]. Plesset and Chapmann [54] proposed a well-known theory to determine the microjet velocity, expressed as

$$v_j = 8.97(\frac{H}{R_0})^2 \sqrt{\frac{P_\infty - P_v}{\rho_s}} \tag{30}$$

The microjet is impeded by the abrasive and will simultaneously stress and damage the abrasive. Diamond abrasive is generally hard and can be approximated as rigid bodies, therefore the deformation and wear of abrasive is ignored in this paper. The microjet pressure can be expressed as according to the water hammer pressure from the literature [53,55].

$$P_j = v_j \frac{\rho_s c_s \rho_a c_a}{\rho_s c_s + \rho_a c_a} \tag{31}$$

where, H is the distance between the center of the bubble and the wall. Substituting Eqs. (21–31) into Eq. (20), the abrasive particle velocity can be solved and further calculate the kinetic energy of free abrasive particle. Table 1 lists the used relevant model conditions with reference to previous literature [34–43].

3. Results and discussion

3.1. Displacement characteristics of fixed abrasive in UP

The force curves on the polishing tool with time under the action of ultrasonic vibration with different ultrasonic parameters is shown in Fig. 3 (A, B). The force on the polishing tool follows the ultrasonic vibration to show a periodic variation behavior, with the mean value of the fluctuation and the preloading force in agreement. With the increase of ultrasonic amplitude, the amplitude of force fluctuation increases. With the increase of ultrasonic frequency, the amplitude of force fluctuation remains the constant, while the period of force fluctuation becomes shorter. Fig. 3 (C) shows the effect of preloading force on the average gap using polishing pads of different surface roughness R_{qp}

Table 1
The used relevant model conditions [34–43].

Conditions	Parameters
Cavitation model	$P_0 = 0.1013$ Mpa; $P_v = 2330$ Pa; $\mu = 0.001$ Pa s; $\sigma = 0.0725$ N/m; $\gamma = 4/3$; $k = 1$; $h_i = R_0/8.54$; $k_1 = 5190$ m/s; $k_2 = 25306$ m/s; $C = 200$
Initial bubble radius	$R_0 = 5$–25 μm
Ultrasonic	$f = 20$–60 kHz; $A = 0.6$–1.5 μm; $\varphi_0 = 0$
Workpiece (SiC)	$\rho_w = 3120$ kg/m³; $c_w = 5482$ m/s; $H_w = 2840$ kg/mm²; $E_w = 410$ Mpa; $\nu_w = 0.16$
Pad (PU)	$\rho_p = 490$ kg/m³; $c_p = 1900$ m/s; $E_p = 2.29$ Mpa; $\nu_p = 0.47$; $R_p = 5$ mm; $L = 3$ mm; $\rho_{pa} = 13.5$ mm⁻¹; $R_{qp} = 13.13$–53.6 μm; $R_{pa} = 37$ μm
Abrasive (Diamond)	$\rho_a = 3520$ kg/m³; $c_a = 36000$ m/s; $E_a = 1000$ Gpa; $\nu_a = 0.07$
Polishing slurry	$\rho_s = 1200$ kg/m³; $c_s = 1500$ m/s
Abrasive size	$d_a = 5$–25 μm
Preloading force	$F_0 = 5$–25 N

value. When the roughness R_{qp} value is determined, the average gap decreases with increasing preloading force. In addition, the average gap becomes larger with increasing R_{qp} value for a certain preloading force, and the average gap varies significantly with the preloading force using a rough pad with a larger roughness R_{qp} value. Considering the dynamic

physical effect of ultrasonic vibration, the gap also exhibits a dynamic variation regulation, as shown in Fig. 3 (D). It can be found that when a preloading force of 5 N is applied, the average gap without ultrasonic vibration is equal to 2.868 μm. The dynamic gap fluctuates between the maximum gap value of 3.021 μm and the minimum gap value of 2.718 μm under the ultrasonic vibration with an amplitude of 1.5 μm and a frequency of 20 kHz. Meanwhile, the maximum profile peak height of the positive direction of dynamic gap is larger than the maximum profile valley depth of the negative direction of dynamic gap, which may be attributed to the compressive properties of the elastomer material. Further, Fig. 3 (E) shows the effect of contact gap on the indentation depth of a single fixed abrasive particle using different abrasive size values. The solidified abrasive is constricted between the polishing pad and the workpiece as a whole, there is no relationship between the indentation depth and the preloading force, thus the application of ultrasonic vibration does not change the indentation depth of the sandwiched abrasive owing to the identical contact gap at a specified position. Furthermore, the indentation depth of fixed abrasive depends mainly on the abrasive geometry, which is related to the abrasive size and contact gap, and exists only within twice the contact gap of the abrasive size. As the contact gap increases and the abrasive size decreases, the indentation depth of the fixed abrasive gradually decreases.
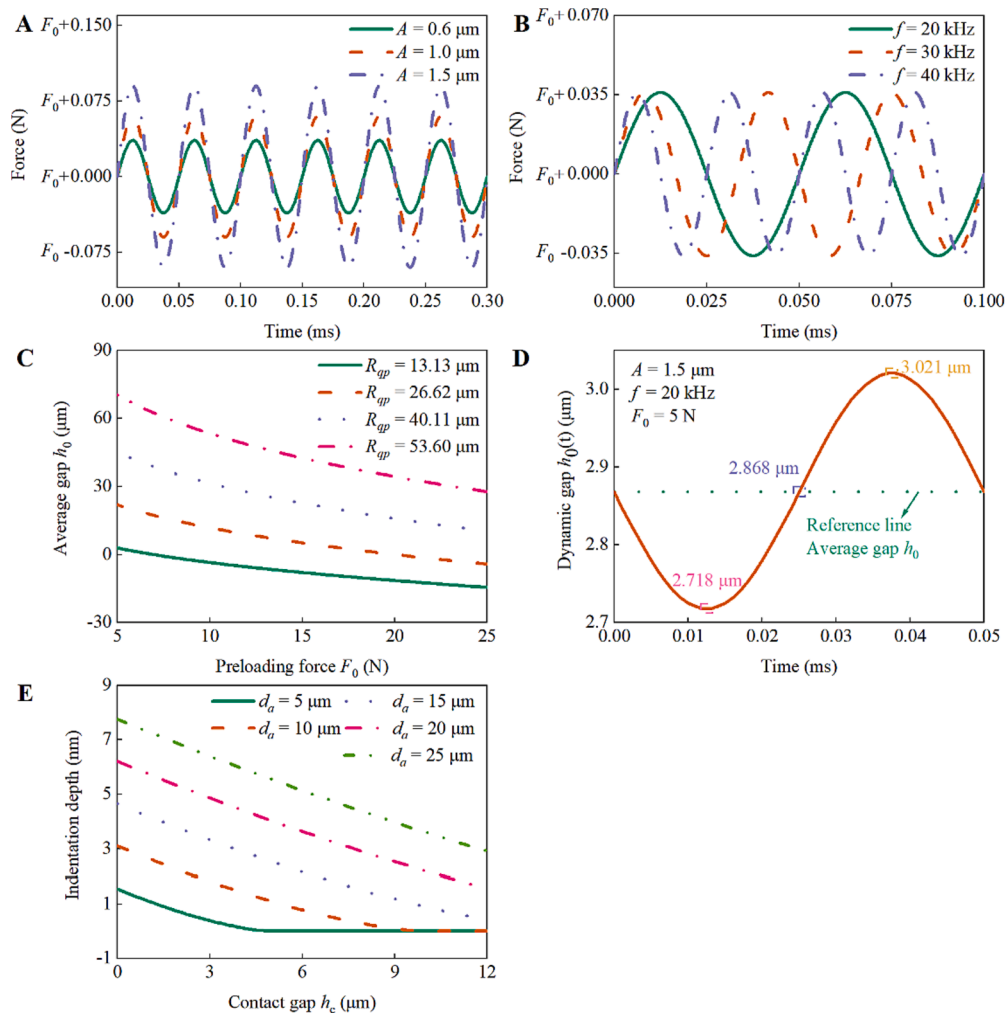

Fig. 3. The force curves on the polishing tool with time under the action of ultrasonic vibration with different ultrasonic amplitude (A) and ultrasonic frequency (B); (C) effect of preloading force on the average gap using polishing pads of different surface roughness R_{qp} value; (D) the dynamic gap curve with time for an ultrasonic cycle with a preloading force of 5 N, an ultrasonic amplitude of 1.5 μm, and a frequency of 20 kHz; (E) effect of contact gap on the indentation depth of single fixed abrasive particle using different abrasive size values.

3.2. Bubble characteristics in UP

Relative radius (*RR*), defined as the ratio of bubble radius after cavitation for a specific time to the initial bubble radius, was used to indicate the cavitation oscillation process quantitatively. Fig. 4 shows the relative radius curves of cavitation bubble with time oscillated at different conditions parameters. Under the action of ultrasonic waves, cavitation bubbles with various dimensions emerge in the polishing solution, and these cavitation bubbles exhibit the similar acoustic regulation, displaying a non-linear vibration with periodicity. Influenced by the driving acoustic pressure, the cavitation bubble experienced growth and expansion to the maximum radius before starting to compress and then entering the collapse stage. Fig. 4(A) indicates that as the initial cavitation bubble radius increases, the oscillation period increases slightly and is relatively similar, whereas the maximum *RR* value first drops rapidly and then stabilizes. Fig. 4(B) demonstrates that a smaller ultrasonic amplitude makes a smaller maximum *RR* value and a smaller oscillation period, indicating a smaller bubble cavitation effect. Moreover, when the ultrasonic amplitude is 0.6 μm or 0.7 μm, the generated ultrasonic sound pressure amplitude is 92.53 kPa and 107.95 kPa, similar to the cavitation threshold P_{ct} of 104.31 kPa calculated

according to Eq. (32), which is the main reason for the depressed cavitation effect.

$$P_{ct} = P_0 - P_v + \frac{2\sqrt{3}}{9} \left(\frac{(2\sigma/R_0)^3}{P_0 - P_v + 2\sigma/R_0} \right)^{1/2} \tag{32}$$

According to Eq. (19), it can be found that the ultrasonic sound pressure amplitude is also influenced by the ultrasonic frequency, as shown in Fig. 4(C). When the frequency varies from 20 kHz to 60 kHz, the ultrasonic sound pressure amplitude also increases, and the maximum value of relative radius first increases and then stabilizes, indicating that a greater ultrasonic sound pressure amplitude helps to enhance the cavitation effect when it is controlled within a certain limit, while the cavitation effect will no longer be enhanced when its value exceeds this limit. Meanwhile, as the frequency increases, the oscillation period is significantly shortened, which can also be clearly seen in Fig. 4 (D). It can also be found that when the frequency increases at a specific ultrasonic sound pressure amplitude, the relative radius maximum decreases, i.e., the cavitation effect is instead weakened. This is because the negative pressure stage is shortened at high frequency, causing the cavitation bubble to not fully complete the growth and expansion process, meaning that the radius becomes smaller, the collapse process is
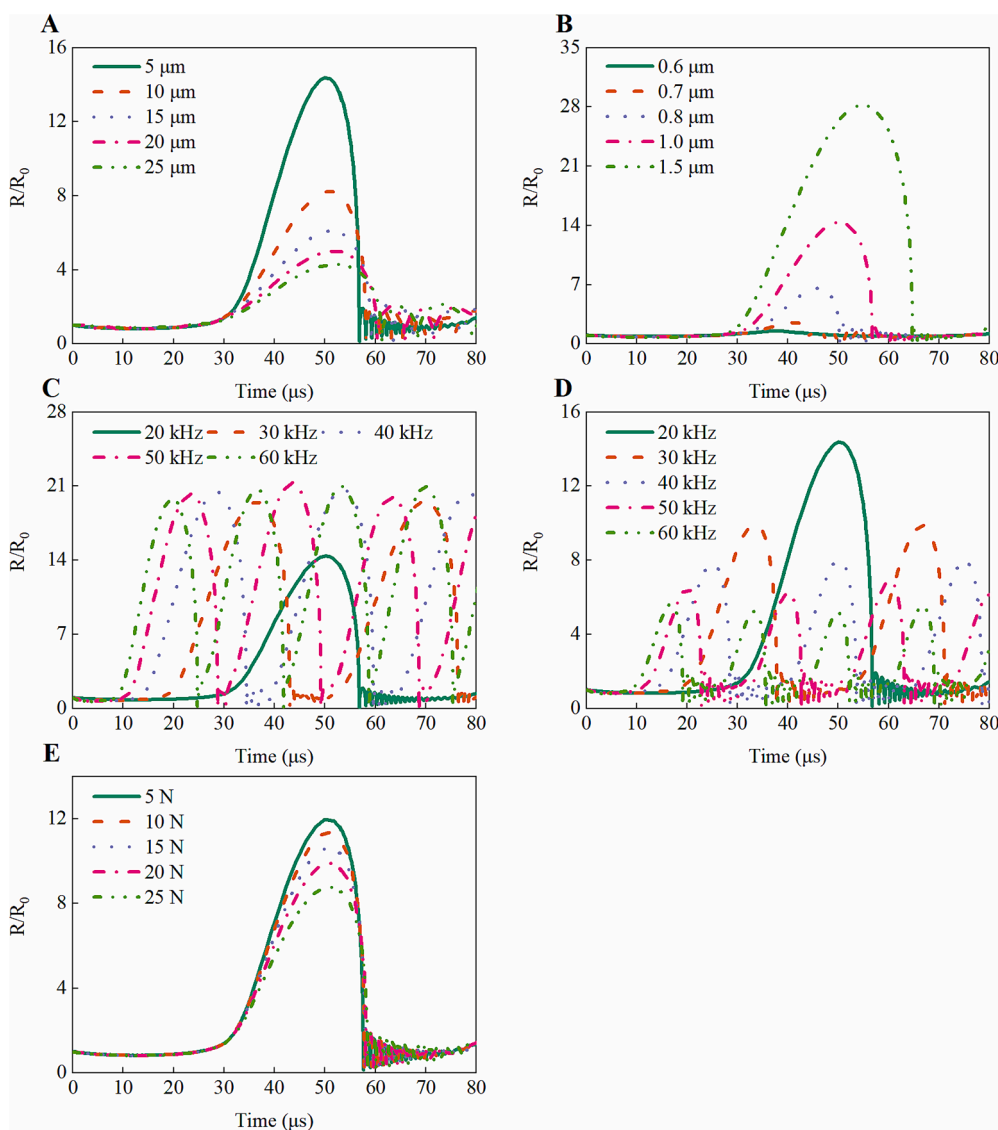

Fig. 4. The *RR* curves of cavitation bubble with time oscillated at different conditions parameters: (A) initial cavitation bubble radius, (B) ultrasonic amplitude, (C) ultrasonic frequency at variable ultrasonic sound pressure amplitude, (D) ultrasonic frequency at a specific ultrasonic sound pressure amplitude, (E) preloading force.

reduced, and the cavitation strength is decremented [56]. Integrating the results of Fig. 4(C, D), the ultrasonic amplitude and frequency are controlled at 1.5 μm and 30 kHz can achieve the optimal bubble oscillation results in ultrasonic processing. Fig. 4(E) shows that the increasing preloading force only slightly decreases the maximum *RR* value, indicating that the bubble cavitation effect is attenuated in the appropriate range near the workpiece wall.

3.3. Impact characteristics of free abrasive in UP

In the auxiliary processing of ultrasonic free abrasives, the regular oscillation of the bubbles is the dominant contributor to the abrasive impact. It is defined the cavitation effect in the form of microjet and shockwave generated when the rupture of the bubble occurs. It is seen in Fig. 4 that the bubble basically ruptures at the relative radius of 0.1–0.3, and the bubble basically produces stronger microjets at the relative radius of 1–2 through the literature [57–59]. Fig. 5 gives the effect of relative radius on the different simulation target results for the corresponding relative radius range. As the relative radius increases from 1 to 2, the microjet velocity increases in the range of approximately 130.3–521.2 m/s, the microjet pressure increases in the range of approximately 231.3–925 MPa, and the impact kinetic energy generated by the microjet induced abrasive is also increased from 0.222 nJ to 0.888 nJ, as shown in Fig. 5(A, C). The similar bubble break-up velocities are obtained by Eq. (27), about 92.91–518.23 m/s. In addition, Fig. 5(B, D) also shows the pressure and velocity generated by the shock wave in the range of 1583–1890 MPa and 1695–2546 m/s, respectively. Also, the impact kinetic energy of the shock wave-induced abrasive varies from 0.217 nJ to 2.477 nJ. All four of them show negative correlation with relative radius, and their variation rates are larger at a smaller relative radius. Compared with the data of previous researches [50,60–63], they used ultrasound, laser or tensile stress wave to generate bubbles to drive the abrasive particle with a radius of 5–50 μm for velocity and kinetic energy tests, and the velocity of abrasives was basically in the range of 20–200 m/s. According to the kinetic energy-velocity transformation, the velocity of abrasives in this paper is basically in the range of 0–150 m/s, which is generally consistent with the previous research results and verifies the validity of the proposed model in this paper.

Fig. 6 shows the effect of ultrasonic amplitude, ultrasonic frequency, particle size, and preloading force on the kinetic energy of single free abrasive particle from the microjet and the shock wave. Firstly, based on the consideration of the impact kinetic energy of abrasive, whether it is shock wave-induced or microjet-induced, ultrasonic amplitude, ultrasonic frequency and abrasive size all contribute positively to the change of the generated impact kinetic energy. The kinetic energy of the abrasive tends to increase roughly linearly with increasing frequency and approximately as a quadratic function with increasing particle size. It is noteworthy that the kinetic energy of the abrasive induced by the shock wave has a cliff-like increment at an amplitude of 0.7–0.8 μm, which is largely ascribed that the ultrasonic sound pressure amplitude generated at a small ultrasonic amplitude does not reach the criterion of cavitation threshold, thus resulting in a weak shock wave. In addition, increasing the preloading force leads to a reduction in the kinetic energy of free abrasive, thereby making the bubble cavitation occur closer to the surround-wall surface, which indicates that the surround-wall surface attenuates the bubble cavitation effect in the proper boundary, further resulting in a reduction in the impact kinetic energy of abrasive, fortunately, the overall variation is relatively slight.

3.4. Abrasive amount characteristics in UP

The entire amount of damage and removal is the accumulation result of a large amount of fixed abrasives scratching and free abrasives impact on the workpiece surface. Fig. 7 shows the effect of preloading force and ultrasonic vibration on the number of abrasive particles in the polishing slurry. From Fig. 7(A), it can be seen that an increase in preloading force leads to a power function growth in the percentage of fixed abrasives and weakening of the percentage of free abrasives. from Fig. 7(B), the fixed abrasives number shows a near-sinusoidal function curve with time under ultrasonic vibration with an amplitude of 1.5 μm. However, compared to the average amount of solidified abrasive without ultrasonic vibration, the fluctuation amplitude distance in the negative direction is larger than that in the positive direction, which reveals the reason why the increase rate of solidified abrasive number slows down as the force becomes larger.
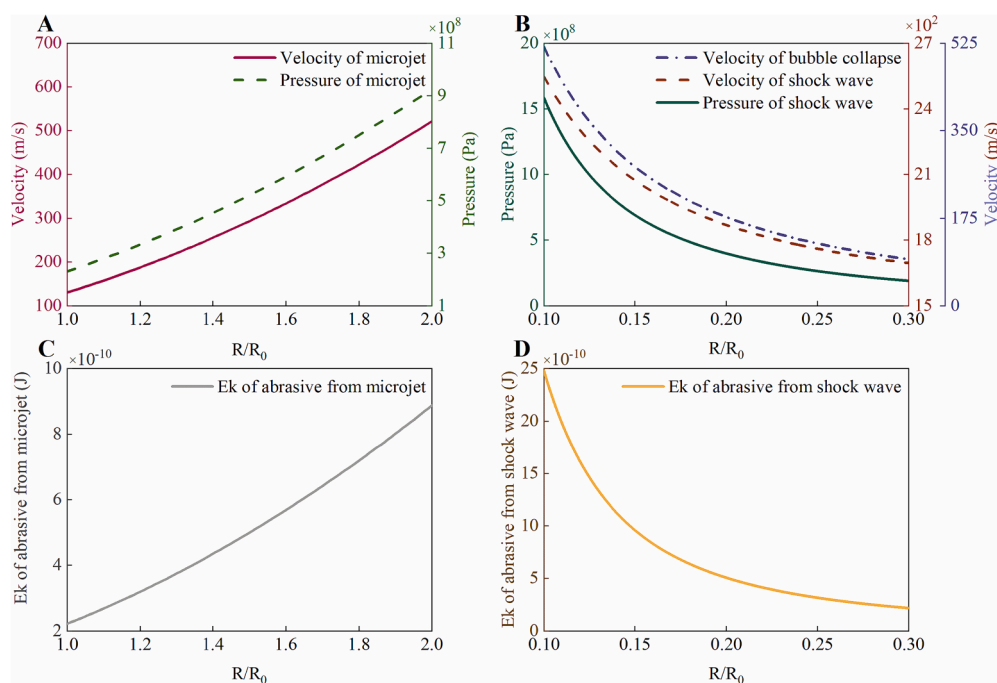

Fig. 5. Effect of relative radius on the different simulation target results: (A) velocity and pressure of the microjet, (B) velocity and pressure of shock wave and the velocity of bubble collapse, (C, D) kinetic energy (Ek) of single free abrasive particle from the microjet and the shock wave, respectively.
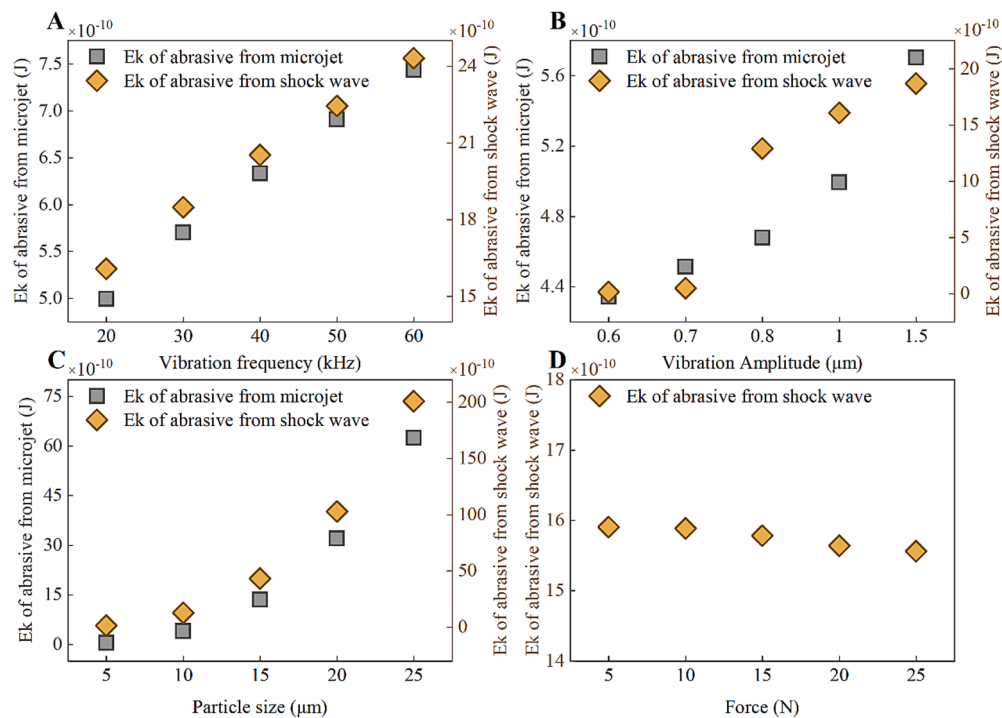
Fig. 6. Effect of (A) ultrasonic amplitude, (B) ultrasonic frequency, (C) particle size, and (D) preloading force on the kinetic energy of single free abrasive particle from the microjet and the shock wave.
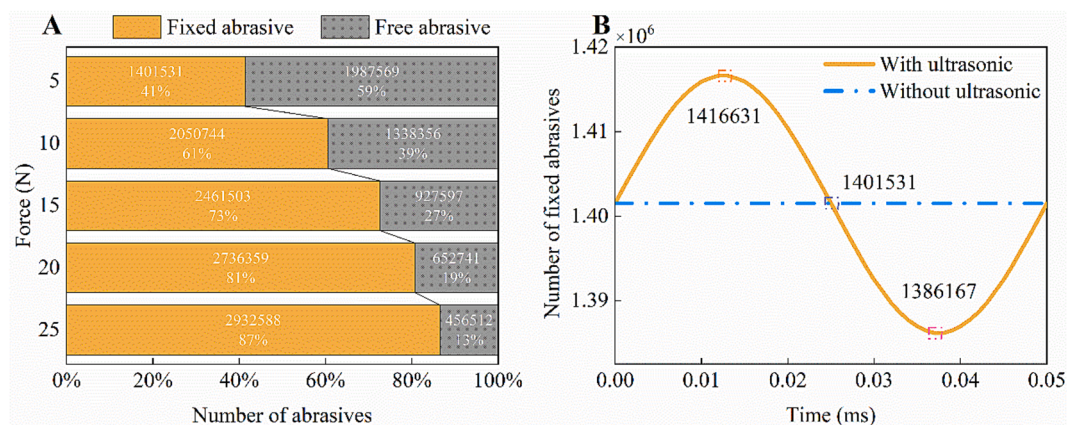

Fig. 7. Effect of (A) preloading force and (B) ultrasonic on the number of abrasive particles in the polishing slurry.

4. Conclusions and future work

In this paper, the novel dynamic indentation depth model of fixed abrasive and impact kinetic energy model of free abrasive were established through mechanical and cavitation theoretical analysis for the ultrasonic polishing of silicon carbide. Numerical simulations and comparisons with previous research studies were conducted to verify the validity of the established model. Some main conclusions and future works are as follows:

1) Under the action of ultrasonic physical vibration, the amount of different types of abrasives and the dynamic gap values change non-sinusoidally, mainly due to the elasticity of the polishing tool. The indentation depth of a fixed abrasive depends mainly on the abrasive geometry. As the contact gap and the abrasive size decrease, the indentation depth decreases gradually.

2) Under the synergistic effect of cavitation-induced shock wave and microjet, the velocity of free abrasive is basically in the range of

0–150 m/s, and the abrasive kinetic energy increases roughly linearly with ultrasonic frequency, approximately as a quadratic function with the increase of particle size.

3) It is noteworthy that the kinetic energy induced by the shock wave has a cliff-like increment at an amplitude of 0.7–0.8 μm, revealing that the abrasive motion occurs significantly only with effective cavitation effects. Increasing the preloading force will lead to a reduction in the kinetic energy of free abrasives, which indicates the surround-wall surface attenuates the bubble cavitation effect.

4) In future work, it is necessary to further investigate the model of abrasives lateral movement and material removal occurring in actual polishing processing based on the interaction idea of particles in elastic–plastic deformation, near-workpiece surfaces, and multi-scale of millimeter, micrometer and nanometer. Further, it is necessary to determine the contribution of ultrasonic to material removal, and to identify the optimal process parameter combination for maximum material removal while ensuring processing accuracy.

CRediT authorship contribution statement

Xin Chen: Conceptualization, Data curation, Formal analysis, Methodology, Software, Validation, Writing – original draft, Writing – review & editing. **Shucong Xu:** Data curation, Formal analysis, Investigation, Software. **Juan Ignacio Ahuir-Torres:** Validation, Writing – review & editing. **Zixuan Wang:** Project administration, Resources, Validation. **Xun Chen:** Supervision, Writing – review & editing. **Tianbiao Yu:** Funding acquisition, Supervision, Writing – review & editing. **Ji Zhao:** Funding acquisition, Project administration, Supervision, Writing – review & editing.

Declaration of competing interest

The authors declare that they have no known competing financial interests or personal relationships that could have appeared to influence the work reported in this paper.

Acknowledgments

References

[1] Z. Xia, F. Fang, E. Ahearne, M. Tao, Advances in polishing of optical freeform surfaces: a review, J. Mater. Process. Technol. 286 (2020), 116828, https://doi.org/10.1016/j.jmatprotec.2020.116828.

[2] X. Wang, W. Zhai, J.Y. Wang, B. Wei, Strength and ductility enhancement of high-entropy FeCoNi2Al0.9 alloy by ultrasonically refining eutectic structures, Scr. Mater. 225 (2023), 115154, https://doi.org/10.1016/j.scriptamat.2022.115154.

[3] T. Yu, Z. Wang, X. Guo, P. Xu, J. Zhao, L. Chen, Effect of ultrasonic vibration on polishing monocrystalline silicon: surface quality and material removal rate, Int. J. Adv. Manuf. Technol. 103 (2019) 2109–2119, https://doi.org/10.1007/s00170-019-03385-y.

[4] X. Yang, X. Yang, K. Kawai, K. Arima, K. Yamamura, Ultrasonic-assisted anodic oxidation of 4H-SiC (0001) surface, Electrochem. Commun. 100 (2019) 1–5, https://doi.org/10.1016/j.elecom.2019.01.012.

[5] M.Y. Tsai, W.Z. Yang, Combined ultrasonic vibration and chemical mechanical polishing of copper substrates, Int. J. Mach. Tools Manuf. 53 (2012) 69–76, https://doi.org/10.1016/j.ijmachtools.2011.09.009.

[6] N. Sihag, P. Kala, P.M. Pandey, Analysis of surface finish improvement during ultrasonic assisted magnetic abrasive finishing on chemically treated tungsten substrate, Procedia Manuf. 10 (2017) 136–146, https://doi.org/10.1016/j.promfg.2017.07.040.

[7] M. Srivastava, P.M. Pandey, The influence of ultrasonic vibrations on material removal in the silicon wafer polishing using DDCAMRF: experimental investigations and process optimization, Proc. Inst. Mech. Eng. Part C J. Mech. Eng. Sci. (2021), https://doi.org/10.1177/09544062211038979.

[8] M. Srivastava, G. Singh, P.M. Pandey, Ultrasonic vibration assisted double disc chemo-magnetorheological finishing of silicon wafer: experimental investigations and optimization for surface roughness, Proc. Inst. Mech. Eng. Part B J. Eng. Manuf. (2023), https://doi.org/10.1177/09544054231178952.

[9] W. Xu, X. Lu, G. Pan, Y. Lei, J. Luo, Effects of the ultrasonic flexural vibration on the interaction between the abrasive particles; Pad and sapphire substrate during chemical mechanical polishing (CMP), Appl. Surf. Sci. 257 (2011) 2905–2911, https://doi.org/10.1016/j.apsusc.2010.10.088.

[10] H. Deng, M. Zhong, W. Xu, Effects of different dispersants on chemical reaction and material removal in ultrasonic assisted chemical mechanical polishing of sapphire, ECS J. Solid State Sci. Technol. 11 (2022), 033007, https://doi.org/10.1149/2162-8777/ac5a6d.

[11] Y. Choopani, M.R. Razfar, M. Khajehzadeh, M. Khosrojerdi, Design and development of ultrasonic assisted-rotational magnetorheological abrasive flow finishing (UA-RMRAFF) process, Appl. Acoust. 197 (2022), 108950, https://doi.org/10.1016/j.apacoust.2022.108950.

[12] P.K. Baghel, V. Mishra, R. Kumar, G.S. Khan, Ultrasonic vibration–assisted magnetorheological hybrid finishing process for glass optics, Int. J. Adv. Manuf. Technol. 125 (2023) 2265–2276, https://doi.org/10.1007/s00170-023-10819-1.

[13] H. Chen, S. Liu, J. Wang, D. Chen, Study on effect of microparticle's size on cavitation erosion in solid-liquid system, J. Appl. Phys. 101 (2007), https://doi.org/10.1063/1.2734547.

[14] G.R. Desale, B.K. Gandhi, S.C. Jain, Particle size effects on the slurry erosion of aluminium alloy (AA 6063), Wear 266 (2009) 1066–1071, https://doi.org/10.1016/j.wear.2009.01.002.

[15] M.K. Padhy, R.P. Saini, Effect of size and concentration of silt particles on erosion of Pelton turbine buckets, Energy 34 (2009) 1477–1483, https://doi.org/10.1016/j.energy.2009.06.015.

[16] Y. Zhang, Y. Zhang, Z. Qian, B. Ji, Y. Wu, A review of microscopic interactions between cavitation bubbles and particles in silt-laden flow, Renew. Sustain. Energy Rev. 56 (2016) 303–318, https://doi.org/10.1016/j.rser.2015.11.052.

[17] C. Haosheng, W. Jiadao, C. Darong, Cavitation damages on solid surfaces in suspensions containing spherical and irregular microparticles, Wear 266 (2009) 345–348, https://doi.org/10.1016/j.wear.2008.05.010.

[18] J.R. Laguna-Camacho, R. Lewis, M. Vite-Torres, J.V. Méndez-Méndez, A study of cavitation erosion on engineering materials, Wear 301 (2013) 467–476, https://doi.org/10.1016/j.wear.2012.11.026.

[19] J.H. Wu, W.J. Gou, Critical size effect of sand particles on cavitation damage, J. Hydrodyn. 25 (2013) 165–166, https://doi.org/10.1016/S1001-6058(13)60350-9.

[20] K.L. Tan, S.H. Yeo, Surface modification of additive manufactured components by ultrasonic cavitation abrasive finishing, Wear 378–379 (2017) 90–95, https://doi.org/10.1016/j.wear.2017.02.030.

[21] K.L. Tan, S.H. Yeo, Surface finishing on IN625 additively manufactured surfaces by combined ultrasonic cavitation and abrasion, Addit. Manuf. 31 (2020), 100938, https://doi.org/10.1016/j.addma.2019.100938.

[22] A.S. Kumar, S. Deb, S. Paul, Ultrasonic-assisted abrasive micro-deburring of micromachined metallic alloys, J. Manuf. Process. 66 (2021) 595–607, https://doi.org/10.1016/j.jmapro.2021.04.019.

[23] C. Peng, Z. Chaoyue, L. Qinfeng, Z. Shilong, S. Yu, L. Hairui, F. Jianhong, Erosion characteristics and failure mechanism of reservoir rocks under the synergistic effect of ultrasonic cavitation and micro-abrasives, Adv. Powder Technol. 32 (2021) 4391–4407, https://doi.org/10.1016/j.apt.2021.09.046.

[24] F. Farbod, B. Pourabbas, Ultrasonic wave effect on PMMA surface, silica nanoparticles assisted erosion, Wear 300 (2013) 105–113, https://doi.org/10.1016/j.wear.2013.01.095.

[25] J. Ge, Y. Ren, C. Li, Z. Li, S. Yan, P. Tang, X. Xu, Q. Wang, Ultrasonic coupled abrasive jet polishing (UC-AJP) of glass-based micro-channel for micro-fluidic chip, Int. J. Mech. Sci. 244 (2023), 108055, https://doi.org/10.1016/j.ijmecsci.2022.108055.

[26] X. Liu, J. Wang, D. Teng, P.J. Liew, C. Huang, Electrorheological fluid–assisted ultrasonic polishing for IN625 additively manufactured surfaces, Int. J. Adv. Manuf. Technol. 120 (2022) 891–905, https://doi.org/10.1007/s00170-022-08838-5.

[27] T. Zhang, Z. Wang, T. Yu, H. Chen, J. Dong, J. Zhao, W. Wang, Modeling and prediction of generated local surface profile for ultrasonic vibration-assisted polishing of optical glass BK7, J. Mater. Process. Technol. 289 (2021), 116933, https://doi.org/10.1016/j.jmatprotec.2020.116933.

[28] V.L. Popov, Contact Mechanics and Friction - Hertz Force (2017). http://www.springerlink.com/index/10.1007/978-3-642-10803-7.

[29] J.A. Greenwood, J.B.P. Williamson, Contact of nominally flat surfaces, Proc. R. Soc. London. Ser. A. Math. Phys. Sci. 295 (1966) 300–319, https://doi.org/10.1098/rspa.1966.0242.

[30] D. Liu, R. Yan, T. Chen, Material removal model of ultrasonic elliptical vibration-assisted chemical mechanical polishing for hard and brittle materials, Int. J. Adv. Manuf. Technol. 92 (2017) 81–99, https://doi.org/10.1007/s00170-017-0081-z.

[31] J.Z. Jiang, Y.W. Zhao, Y.G. Wang, J. Bin Luo, A chemical mechanical polishing model based on the viscous flow of the amorphous layer, Wear 265 (2008) 992–998, https://doi.org/10.1016/j.wear.2008.02.006.

[32] Y. Zhao, L. Chang, A micro-contact and wear model for chemical–mechanical polishing of silicon wafers, Wear 252 (2002) 220–226, https://doi.org/10.1016/S0043-1648(01)00871-7.

[33] A. Lu, T. Jin, Q. Liu, Z. Guo, M. Qu, H. Luo, M. Han, Modeling and prediction of surface topography and surface roughness in dual-axis wheel polishing of optical glass, Int. J. Mach. Tools Manuf. 137 (2019) 13–29, https://doi.org/10.1016/j.ijmachtools.2018.10.001.

[34] U. Parlitz, V. Englisch, C. Scheffczyk, W. Lauterborn, Bifurcation structure of bubble oscillators, J. Acoust. Soc. Am. 88 (1990) 1061–1077, https://doi.org/10.1121/1.399855.

[35] W. Yao, Q. Chu, B. Lyu, C. Wang, Q. Shao, M. Feng, Z. Wu, Modeling of material removal based on multi-scale contact in cylindrical polishing, Int. J. Mech. Sci. 223 (2022), 107287, https://doi.org/10.1016/j.ijmecsci.2022.107287.

[36] C. Zhang, Y. Liang, Z. Cui, F. Meng, J. Zhao, T. Yu, Study on the effect of ultrasonic vibration-assisted polishing on the surface properties of alumina ceramic, Ceram. Int. 48 (2022) 21430–21447, https://doi.org/10.1016/j.ceramint.2022.04.105.

[37] X. Chen, C. Zhang, F. Meng, T. Yu, J. Zhao, Polishing mechanism analysis of silicon carbide ceramics combined ultrasonic vibration and hydroxyl, Tribol. Int. 179 (2023), 108187, https://doi.org/10.1016/j.triboint.2022.108187.

[38] X. Chen, Y. Liang, Z. Cui, F. Meng, C. Zhang, L. Chen, T. Yu, J. Zhao, Study on material removal mechanism in ultrasonic chemical assisted polishing of silicon carbide, J. Manuf. Process. 84 (2022) 1463–1477, https://doi.org/10.1016/j.jmapro.2022.11.014.

[39] M. Li, J. Xie, Green-chemical-jump-thickening polishing for silicon carbide, Ceram. Int. 48 (2022) 1107–1124, https://doi.org/10.1016/j.ceramint.2021.09.196.

[40] M. Ida, Bubble-bubble interaction: a potential source of cavitation noise, Phys. Rev. E - Stat. Nonlinear, Soft Matter Phys. 79 (2009) 1–7, https://doi.org/10.1103/PhysRevE.79.016307.

[41] K. Trachenko, B. Monserrat, C.J. Pickard, V.V. Brazhkin, Speed of sound from fundamental physical constants, Sci. Adv. 6 (2020) 1–6, https://doi.org/10.1126/sciadv.abc8662.

[42] F. Li, J. Cai, X. Huai, B. Liu, Interaction mechanism of double bubbles in hydrodynamic cavitation, J. Therm. Sci. 22 (2013) 242–249, https://doi.org/10.1007/s11630-013-0619-9.

[43] S. Behnia, A.J. Sojahrood, W. Soltanpoor, L. Sarkhosh, Towards classification of the bifurcation structure of a spherical cavitation bubble, Ultrasonics 49 (2009) 605–610, https://doi.org/10.1016/j.ultras.2009.05.005.

[44] J. Stella, R. Alcivar, Influence of addition of microsized alumina particles on material damage induced by vibratory cavitation erosion, Wear 436–437 (2019), 203027, https://doi.org/10.1016/j.wear.2019.203027.

[45] P.P. Gohil, R.P. Saini, Coalesced effect of cavitation and silt erosion in hydro turbines - a review, Renew. Sustain. Energy Rev. 33 (2014) 280–289, https://doi.org/10.1016/j.rser.2014.01.075.

[46] P.J. Dunstan, S.C. Li, Cavitation enhancement of silt erosion: numerical studies, Wear 268 (2010) 946–954, https://doi.org/10.1016/j.wear.2009.12.036.

[47] R. Timm, Optical and acoustic investigations of the dynamics of laser-produced cavitation bubbles near a solid boundary, J. Fluid Mech. 206 (1989) 299–338, https://doi.org/10.1017/S0022112089002314.

[48] E.A. Brujan, Shock wave emission from laser-induced cavitation bubbles in polymer solutions, Ultrasonics 48 (2008) 423–426, https://doi.org/10.1016/j.ultras.2008.02.001.

[49] M.H. Rice, J.M. Walsh, Equation of state of water to 250 kilobars, J. Chem. Phys. 26 (1957) 824–830, https://doi.org/10.1063/1.1743415.

[50] Y. Fu, X. Zhu, J. Wang, T. Gong, Numerical study of the synergistic effect of cavitation and micro-abrasive particles, Ultrason. Sonochem. 89 (2022), 106119, https://doi.org/10.1016/j.ultsonch.2022.106119.

[51] E.A. Brujan, T. Ikeda, K. Yoshinaka, Y. Matsumoto, The final stage of the collapse of a cloud of bubbles close to a rigid boundary, Ultrason. Sonochem. 18 (2011) 59–64, https://doi.org/10.1016/j.ultsonch.2010.07.004.

[52] A. Vogel, S. Busch, U. Parlitz, Shock wave emission and cavitation bubble generation by picosecond and nanosecond optical breakdown in water, J. Acoust. Soc. Am. 100 (1996) 148–165, https://doi.org/10.1121/1.415878.

[53] P.A. Lush, Impact of a liquid mass on a perfectly plastic solid, J. Fluid Mech. 135 (1983) 373–387, https://doi.org/10.1017/S0022112083003134.

[54] R.B.C. Milton, S. Plesset, Collapse of an initially spherical vapor cavity in the neighborhood of a solid boundary, J. Fluid Mech. 47 (1971) 283–290, https://doi.org/10.1017/S0022112071001058.

[55] A. Philipp, W. Lauterborn, Cavitation erosion by single laser-produced bubbles, J. Fluid Mech. 361 (1998) 75–116, https://doi.org/10.1017/S0022112098008738.

[56] L. Ye, X. Zhu, Y. Liu, Numerical study on dual-frequency ultrasonic enhancing cavitation effect based on bubble dynamic evolution, Ultrason. Sonochem. 59 (2019), 104744, https://doi.org/10.1016/j.ultsonch.2019.104744.

[57] X. Wang, G. Wu, X. Zheng, X. Du, Y. Zhang, Theoretical investigation and experimental support for the cavitation bubble dynamics near a spherical particle based on Weiss theorem and Kelvin impulse, Ultrason. Sonochem. 89 (2022), 106130, https://doi.org/10.1016/j.ultsonch.2022.106130.

[58] F. Zhao, Q. Yan, D. Cheng, Numerical study on the desorption processes of oil droplets inside oil-contaminated sand under cavitation micro-jets, Ultrason. Sonochem. 78 (2021), 105745, https://doi.org/10.1016/j.ultsonch.2021.105745.

[59] H. Wu, H. Zheng, Y. Li, C.D. Ohl, H. Yu, D. Li, Effects of surface tension on the dynamics of a single micro bubble near a rigid wall in an ultrasonic field, Ultrason. Sonochem. 78 (2021), 105735, https://doi.org/10.1016/j.ultsonch.2021.105735.

[60] M. Arora, C.D. Ohl, K.A. Mørch, Cavitation inception on microparticles: a self-propelled particle accelerator, Phys. Rev. Lett. 92 (2004) 1–4, https://doi.org/10.1103/PhysRevLett.92.174501.

[61] B.M. Borkent, M. Arora, C.D. Ohl, N. De Jong, M. Versluis, D. Lohse, K.A. Mørch, E. Klaseboer, B.C. Khoo, The acceleration of solid particles subjected to cavitation nucleation, J. Fluid Mech. 610 (2008) 157–182, https://doi.org/10.1017/S002211200800253X.

[62] S.J. Doicrycz, K.S. Suslick, Interparticle collisions driven by ultrasound, Science (80). 247 (1990) 1067–1069. https://doi.org/10.1126/science.2309118.

[63] K.L. Tan, S.H. Yeo, Velocity estimation of micro-particles driven by cavitation bubble collapses through controlled erosion experiments, Int. J. Multiph. Flow. 127 (2020), 103271, https://doi.org/10.1016/j.ijmultiphaseflow.2020.103271.